HHS Public Access

Author manuscript

Cancer Res. Author manuscript; available in PMC 2020 April 01.

Published in final edited form as:

Cancer Res. 2019 April 01; 79(7): 1681–1695. doi:10.1158/0008-5472.CAN-18-2602.

Metastatic Tumor-In-A-Dish, A Novel Multi-Cellular Organoid To Study Lung Colonization and Predict Therapeutic Response

Prabhu Ramamoorthy[1,2], **Sufi Mary Thomas**[1,3], **Gaurav Kaushik**[2], **Dharmalingam Subramaniam**[1,2], **Katherine M. Chastain**[4], **Animesh Dhar**[1], **Ossama Tawfik**[5], **Anup Kasi**[6], **Weijing Sun**[6], **Satish Ramalingam**[1], **Sumedha Gunewardena**[7], **Shahid Umar**[2], **Joshua M. Mammen**[2], **Subhash B. Padhye**[8], **Scott J. Weir**[9], **Roy A. Jensen**[5], **G. Sitta Sittampalam**[10], and **Shrikant Anant**[1,2,*]

[1]Department of Cancer Biology, University of Kansas Medical Center, Kansas City, KS 66160.

[2]Department of General Surgery, University of Kansas Medical Center, Kansas City, KS 66160.

[3]Department of Otolaryngology, University of Kansas Medical Center, Kansas City, KS 66160.

[4]Department of Pediatrics, Children's Mercy Hospitals and Clinics, Kansas City, MO 64108.

[5]Department of Pathology and Laboratory Medicine, University of Kansas Cancer Center, Kansas City, KS 66160.

[6]Department of Internal Medicine, University of Kansas Medical Center, Kansas City, KS 66160.

[7]Department of Molecular and Integrative Physiology, University of Kansas Medical Center, Kansas City, KS 66160.

[8]Interdisciplinary Science and Technology Research Academy, University of Pune, Pune 411001, India

[9]Department of Pharmacology, Toxicology and Therapeutics, University of Kansas Medical Center, Kansas City, KS 66160.

[10]National Center for Advancing Translational Sciences, NIH, Bethesda, MD 20892.

Abstract

Metastasis is a major cause of cancer-related deaths. A dearth in preclinical models that recapitulates the metastatic microenvironment has impeded the development of therapeutic agents that are effective against metastatic disease. Since the majority of solid tumors metastasize to the lung, we developed a multi-cellular lung organoid that mimics the lung microenvironment with air sac like structures and production of lung surfactant protein. We used these cultures called primitive lung-in-a-dish (PLiD), to recreate metastatic disease using primary and established cancer cells. The metastatic tumor-in-a-dish (mTiD) cultures resemble the architecture of metastatic tumors in the lung including angiogenesis. Pretreating PLiD with tumor exosomes enhanced cancer cell colonization. We next tested the response of primary and established cancer

[*]**Corresponding author:** Shrikant Anant; Department of Cancer Biology 3901 Rainbow Blvd MS1071 Kansas City, KS 66160; Tel: 913-945-6334;, sanant@kumc.edu.

Conflicts of interests: The authors have no financial disclosures. This work is patented to SA, PR, SR and GSS (In vitro Tumor in a Dish and Methods, Patent number 9494573).

cells to current chemotherapeutic agents and an anti-VEGF antibody in mTiD against cancer cells in 2-dimensional (2D) or 3D cultures. The response of primary patient-derived colon and ovarian tumor cells to therapy in mTiD cultures matched the response of the patient in the clinic, but not 2D or single cell type 3D cultures. The sensitive mTiD cultures also produced significantly lower circulating markers for cancer similar to that seen in patients that responded to therapy. Thus, we have developed a novel method for tumor colonization *in vitro*, a final stage in tumor metastasis. Moreover, the technique has significant utility in precision/personalized medicine, wherein this phenotypic screen can be coupled with current DNA pharmacogenetics to identify the ideal therapeutic agent, thereby increasing the probability of response to treatment while reducing unnecessary side effects.

Introduction

Post-cancer survival has improved dramatically in the last few decades, in part due to early diagnoses, improvement in imaging techniques, radiation therapy, and chemotherapy regimens (1). Therapeutic discovery has been slow, especially for metastatic cancers begging the question of whether we are using the preclinical models that closely represent the primary tumor to test oncology drugs. A significant hindrance to the discovery of new cancer therapies is that current screening methods are poorly predictive of the clinical efficacy and safety of drug candidates.

The applicability of two-dimensional (2D) cultures, which along with murine models has been the mainstay of basic cancer biology research, has become increasingly called into question (2). Despite rapid advances in the ability to screen large libraries of compounds, there has not been a corresponding increase in the number of approved drugs that had been expected from such large screens using 2D cultures followed by 3-dimensional (3D) spheroid culture and animal models to select clinical candidates (3). An advantage of the 3D system is the cell to cell communication between cancer cells affecting how cells react to therapeutic agents (4). However, a significant disadvantage is the lack of complete tumor microenvironment including the stroma and vasculature. This reflects the inadequacy of current culture systems that does not correlate clinically to predict chemoresistance or propensity for metastasis. Hence, developing an *in vitro* model to better represent a more physiologically relevant system, one that uses healthy cells as a matrix, to model the development, colonization and response of metastatic tumors to treatment is essential. While modeling ‘mini’ healthy organs has been fast paced and prolific, efforts to model various solid tumors and their microenvironment have been lacking. Further improvement in organoids will allow advance understanding of hypoxia, metastasis, treatment effects, and drug resistance at the cellular level (5). We have now combined the progress made in modeling healthy organelles in organoid culture, and introduced tumor cells, creating an organoid system that recapitulates the tumor microenvironment with surrounding healthy tissue.

Using a combination of commercially available cell lines and primary patient-derived cells, we created a lung organoid *in vitro,* which we have named “primitive lung-in-a-dish” (PLiD). We then grew commercially available colon or ovarian cancer cell lines in PLiD and

named it “metastatic tumor-in-a-dish” (mTiD). This model now represents the metastatic potential of tumor cells *in vitro*. Using this model, we tested the therapeutic efficacy of several standard of care chemotherapeutic agents. Further, we used primary patient-derived colon or ovarian tumor cells and corroborated the patient’s response to therapy with that of the mTiD cultures *in vitro*. Thus, we have now developed a novel platform with which to screen drug responses, not only for novel therapeutics, but also to optimize a precision approach where a patient’s tumor can be quickly tested in a mTiD system for effective chemotherapeutics.

Materials and Methods

Cell lines and Reagents

Human normal lung epithelial cells (NL20, ATCC, Manassas, VA) were cultured using airway epithelial cell basal medium containing Bronchial epithelial growth kit (ATCC, Manassas, VA). Human normal lung fibroblast (MrC5, ATCC, Manassas, VA) were grown in Fibroblast basal media containing 10% FBS. Human umbilical vein endothelial cells and human normal lymphatic endothelial cells were grown in endothelial basal medium (EBM, Lonza, Allendale, NJ) containing endothelial growth factor (EGM-2 bullet kit, Lonza, Allendale, NJ). The cancer cell lines were obtained from ATCC and cultured in appropriate media. A2780 and cisplatin resistant A2780/C30 were gifted by Dr. Andrew Godwin. The established cell lines were validated by STR analyses. For 2D culture, cells were trypsinized and plated in the adherent cell culture treated plate. Single cell organoids were grown using DMEM containing rhEGF (20ng/ml), rhFGF (20ng/ml), 1X B27, and Heparin calcium salt (0.4%) from ThermoFisher Scientific, Grand Island, NY) in ultra-low attachment plates (Corning, Tewksbury, MA). All the compounds were obtained from Tocris Bioscience (Minneapolis, MN) or Sigma-Aldrich (St Louis, MO). Bevacizumab was obtained from BioRad (Hercules, CA).

Peripheral blood mononuclear cells (PBMCs) isolation

PBMC were isolated from fresh blood using Ficoll-Paque PLUS (ThermoFisher Scientific, Grand Island, NY). Briefly, Blood was diluted 1:1 ratio in PBS, overlay on top of ficoll-paque and centrifuged at 400g for 30 min at room temperature. The PBMCs were collected from the Ficoll-plasma interface, washed twice with PBS at 300 x g at 4^{O}C, and then labeled with PKH26 dye as previously described (6). Fluorescence Z-stack images were captured with a Nikon Eclipse Ti Epi-fluorescent microscope connected with Nikon intensilight C-HGFIE (Nikon, Melville, NY) with ProScan H31 controller (Prior, Rockland, MA).

Patient derived human cancer cells

De-identified tissue explants were collected with informed written consent from patients under the auspices of the University of Kansas Medical Center Biospecimen Repository Core Facility. All protocols for collection of sample in accordance with recognized ethical guidelines (Declaration of Helsinki, Belmont Report, and U.S. Common Rule) by the Human Subject Committee at the University of Kansas Medical Center. Patient characteristics are listed in Supplementary Table S1. Briefly, tumor and ascitic fluid samples from 4 patients were used in this study. Primary colon cancer cells were derived from a

female (hCol1) and a male (hCol2) patient. The patient was administered a combination of Avastin/Bevacizumab, 5-FU, leucovorin, irinotecan capecitabine and oxaliplatin. Tissue from two ovarian cancer patients were acquired in the study. The hOVR1 cultures were derived from primary tumor tissue explants from a patient with clear cell adenocarcinoma of the ovary. The patient was treated with taxol and cisplatin. Unfortunately, the patient had progressive disease and the chemotherapeutic agent was changed to doxorubicin. The hOVR2 cancer cells were cultured from ascites fluid from a patient with adenocarcinoma of the ovary. The patient was treated with taxol and carboplatin, but recurred and was treated with the same regimen.

For human colon cancer tissue, tissue was washed with sterile PBS and minced into small piece. Minced tissue pieces were incubated with collagenase (Type IV, Sigma), for 10–20 min. The resultant cell suspension was passed through a fine fire polished glass pipette to generate a single cell suspension. Cells were subjected to centrifugation at 3000 rpm for 2 m. The cell pellet was suspended in specialized media (spMedia, DMEM containing 20% FBS, hydrocortisone (1μg/ml), rhFGF (5ng/ml), rhEGF (5ng/ml), VEGF (5ng/ml), R3-IGF-1 (15ng/ml), Ascorbic acid (50μg/ml), 2% FBS and 1% Gentamicin, Amphotericin-B). Human ovarian cancer cells from ascitic fluid were cultured in CTC Enrichment cocktail containing anti-CD36 antibody (STEMCELL Technologies Inc., Cambridge, MA) according to the manufacturer's instructions. Briefly, ascitic fluid was incubated with antibody cocktail (RosetteSepTM CTC Enrichment Cocktail, STEMCELL Tech). in the ratio of 50μl/ml for 20 min at RT. The suspension was then diluted (1:1) with PBS containing 2% FBS and cells were separated using density gradient medium, Ficoll-plaque (GE healthcare Life sciences, Pittsburgh, PA). Cells were washed twice in PBS containing 5% FBS at 300g for 10min and cultured in spMedia.

Transduction

Cell lines and patient-derived cells were grown in a humidified incubator at 37°C with 5% CO2. GFP overexpressing plasmids were generated using the pLVX Tet-On Advanced plasmid system (ClonTech Laboratories Inc., Mountain View, CA). Lentiviral particles were generated using Lenti-X cells transfected with the pGIPZ set of packaging plasmids generously donated by Roy Jensen (University of Kansas Medical Center, Kansas City, KS). HCT 116, SW480 and DLD-1 cells were co-tranduced with pLVX-Tet-On and pLVX-Tight plasmids followed by selection with 1 mg/mL G418 (Mediatech Inc.) and 2 μg/mL puromycin (Life Technologies, Grand Island, NY) for 7 d. Cells were consistently maintained in 500 μg/mL G418 and 1 μg/mL puromycin following selection unless otherwise noted.

Primitive Lung in a Dish (PLiD) and Metastatic Tumor in a Dish (mTiD)

For PLiD cultures, lung epithelial NL20 cells , lung fibroblast MRC5, human umblical vein endothelial HUVEC cells and human lymphatic endothelial HLEC cells were mixed in equal proportions (5000 cells/ml) and cultured in mTiD-spMedia-1 (DMEM containing containing hydrocortisone (0.5μg/ml), rhFGF (3ng/ml), rhEGF (3ng/ml), VEGF (2ng/ml), R3-IGF-1 (5ng/ml), Ascorbic acid (10μg/ml), Extract P (0.1%), plasma protein fraction (0.125%), L-Alanyl-L-Glutamine (2.4mM), rhEGF (5ng/ml), rhInsulin (2μg/ml), 2% FBS and 1%

Penicillin-Streptomycin Single or admixed cultures were plated in ultra-low attachment plates. For mTiD cultures, the cancer cells were mixed in equal proportions to lung epithelial NL20 cells, lung fibroblast MRC5, human umblical vein endothelial HUVEC cells and human lymphatic endothelial HLEC cells. After 3–5 days in cultures, PLiD and mTiD organoids were treated with drug and imaged after 48–72h using light microscope (Jenco International, Inc. Portland, OR) or immunofluorescence (Nikon Eclipse Ti Epi-fluorescent microscope connected with Nikon intensilight C-HGFIE with ProScan H31 controller. IC50 values for the response to therapeutic agents were determined following flow cytometry analyses of the cultures.

DNA extraction and sequencing

Tumor tissue and patient-derived primary tumor cells were submitted to the Genomics Core facility at KUMC. Genomics Core facility performed exome interrogation using the TruSeq Exome Library Prep Kit (Illumina FC-150–1001). Following sequence data collection on the Illumina Compute server (iCompute), the raw base call files (.bcl) are converted to fastq files and de-multiplexed into individual libraries. Data is uploaded to a secure FTP site and sequencing data was analyzed by Bioinformatic core facility, KUMC.

Electron Microscopy

For transmission electron microscopy, tissue or organoid samples were fixed and then dehydrated in a graded series of ethanol for 10 min/each. Samples were then placed into propylene oxide for 20 min followed by a solution of 1:1 propylene oxide:Embed 812 resin (Electron Microscopy Sciences, Fort Washington PA) overnight. Samples were then placed into fresh Embed 812 medium formulation resin mixture for 1 hour. Samples were transferred to molds with fresh resin and cured in a 65ºC oven overnight. Sections were cut and imaged on a JEOL. JEM-1400 TEM.

For scanning electron microscope, organoids were fixed and dehydrated in graded series of ethanol for 5 min/step. After being coated with gold, the organoids were viewed in a Hitachi S-2700 SEM (Hitachi, Inc.).

Exosome isolation

Exosomes were isolated from HCT116 cell culture medium using differential centrifugation method (7). Briefly, HCT116 were cultured in DMEM containing 10% exosomes-depleted FBS (ThermoFisher Scientific, Grand Island, NY). The culture medium was collected and centrifuged at 3000xg for 10 min to remove all the floating cells and cell debris. Supernatant was collected and centrifuged at 10,000xg for 30 min at 4^{O}C (Sorvall high speed centrifuge, ThermoFisher Scientific, Grand Island, NY). Exosomes containing supernatant was subsequently centrifuged for 60 min at 100,000xg at 4^{O}C (Sorvall ultracentrifuge, ThermoFisher Scientific, Grand Island, NY). The isolated exosomes were washed twice by resuspending in 5 ml PBS and recentrifuged at 100,000xg for 60 min. Then pellet was resuspended in 200 μl of PBS and protein was measured using Bio-Rad protein assay kit.

Cell proliferation assay

Hexosaminidase assay was used to study the effects of various drugs including 5FU, Oxaliplatin, Irinotecan, SN38, cisplatin and carboplatin on proliferation of cancer cells. Cell proliferation was assessed as percent proliferation rate = [(A/B)×100], where A and B are the absorbance of treated and control cells, respectively. Half maximal inhibitory concentration (IC_{50}) was obtained by 50% of cell death after 72 h of treatment by using GraphPad PRISM software (GraphPad Software, Inc.).

3D single cell type spheroid formation assay

3D spheroid formation assay was performed as previously described (8). Briefly, cells were plated in ultralow attachment plates (Corning Inc., Corning, NY) at a density of 5000 cells/ml in DMEM supplemented with rhEGF, rhFGF, and 2% B27 (Life Technologies, Grand Island, NY) and 1% antibiotic-antimycotic (Mediatech Inc. Manassas, VA) at 37°C in a humidified atmosphere containing 5% CO2. For determining therapeutic effects, the spheroids were treated with 1X, 5X, 10X and 25X IC50 of 2D cultures and imaged after 3–5 days.

Immunofluorescence analyses

Organoids were fixed, paraffin embedded and sectioned. The sections were deparaffinized and stained using mouse anti-E-cadherin (610181, BD Biosciences, San Jose, CA), mouse anti-vimentin (sc-6260, Santa Cruz, Dallas, TX), rabbit anti-CD31 (PA5–16301, ThermoFisher Scientific, Grand Island, NY) or rabbit anti-LYVE1 (ab14917, Abcam, Cambridge, MA). Secondary antibodies donkey anti-mouse/rabbit tagged with FITC (Jackson ImmunoResearch, West Grove, PA) or Alexa 488 (ThermoFisher Scientific, Grand Island, NY). For hypoxia detection, organoids were incubated with 100μM hypoxia probe-1 (pimonidazole hydrochloride) for 2 hour at 37ºC, as per the company protocol (Hypoxyprobe™-1 Kit, Hypoxyprobe, Inc., Burlington, MA) and fixed, stained by using anti-pimonidazole mouse antibody and followed by secondary antibody anti-mouse Dylight 549. Images were captured using Nikon Eclipse Ti microscope using NIS element software.

Western blotting

Western blotting was carried out as previously described (8). Briefly, mTiD/PLiD lysates were prepared and quantified by using Bio-Rad protein assay kit (Thermo Scientific., Chicago, IL). Cell lysates were subjected to SDS-PAGE and blotted onto PVDF membrane (EMD Millipore, Danvers, MA), blocked and incubated with primary antibodies (mouse anti-E-cadherin (610181, BD Biosciences, San Jose, CA), mouse anti-vimentin (sc-6260, Santa Cruz, Dallas, TX), rabbit anti-CD31 (PA5–16301, ThermoFisher Scientific, Grand Island, NY), rabbit anti-LYVE1 (ab14917, Abcam, Cambridge, MA), mouse anti-surfactant protein (SP-B, ab3282, or SP-D, ab1778 Abcam, Cambridge, MA), rabbit anti-carcinoembryonic antigen (CEA, ab135781, Abcam, Cambridge, MA), a mouse anti-MUC16 (CA125, ab10029, Abcam, Cambridge, MA) and mouse anti-GAPDH (sc-365062, Santa Cruz, Dallas, TX). Then incubated with appropriate sheep anti-mouse secondary antibodies (NA911V, GE healthcare Life sciences, Pittsburgh, PA) or donkey anti-rabbit (NA934V, GE healthcare Life sciences, Pittsburgh, PA) tagged with HRP. Proteins of

interest were detected using enhanced chemiluminescence system (RPN2106, GE healthcare Life sciences, Pittsburgh, PA or 34095, ThermoFisher Scientific, Grand Island, NY) and imaged on chemiDoc™ XRS with Image lab software (Bio-Rad, Hercules, CA).

Flow cytometry

Cells were dissociated from mTiD culture by trypsin/EDTA for 15–30 min at 37^0C and then cell suspension was centrifuged at 2000 rpm for 2 min. The pellet was washed twice with PBS containing 2% FBS. Percentage of GFP or mCherry positive cells were determined using the Accuri C6 flow cytometer and analyzed by using CFlow Plus software (BD Biosciences, San Jose, CA). For IC_{50} calculations, a plot between the drug concentration vs 50% reduction in GFP positive cells were calculated by using GraphPad PRISM software.

Chemiluminesence immunoassay (CLIA)

The levels of carcinoembryonic antigen (CEA) and cancer antigen 125, CA125 (MUC 16) were detected using a chemiluminescence kit (ABNOVA Corporation, Walnut, CA) according to the manufacturer's instructions. Briefly, mTiD supernatant was centrifuged at 2,000 x g for 10 minutes to remove debris. Supernatants (50µl) were incubated for 2h at 37^oC in antibody coated wells. Chemiluminescence was detected in a microplate reader (BioTek synergy Neo, Winooski, VT) using the Gen5 software. Percent chemiluminescence in test wells was calculated relative to control.

Statistical Analysis:

Student t-tests are used to calculate statistical significance between treatment groups, and data are reported as mean ± standard error of the mean (SEM). Significance between test groups determined by $p<0.05$. Statistical calculations were performed using Microsoft Office Software (version 2013).

Results

Primary Lung-in-a-dish recapitulates lung architecture

Following regional lymph nodes, the lung represents the most frequent site of metastasis for solid tumors (9,10). An *in vitro* model that mirrors the complex microenvironment and architecture of the human lung would enable an accurate assessment of the biology of tumor metastasis to the lung and also facilitate the development of therapeutic agents that specifically abrogate lung metastasis. Further, an *in vitro* lung model would be useful for high throughput screening of effective therapeutic agents. Towards this, we systematically developed culture conditions to grow normal human lung epithelial NL20 cells with other major cell types in the lung including fibroblasts (MrC5), lymphatic (HLEC) and blood vessel (HUVEC) endothelial cells. While individual cell types aggregated to form small spherical clusters, the cells when put together formed a multi-cell type robust organoid that we named Primitive Lung in a Dish (PLiD, Fig 1A, B, Supplementary Fig S1A,B) To demonstrate the persistence of each individual cell type in the multicellular PLiD organoids, we performed immunofluorescence for molecular markers. Epithelial cells make up the majority of PLiD as indicated by the epithelial marker E-Cadherin (Fig 1C). Fibroblasts were also present and dispersed throughout the organoid as indicated by the vimentin

staining. It is of interest that a higher concentration of vimentin is seen at the periphery of the organoid, which is consistent with stromal presence in the region for matrix deposition and increased stability of the organoid. Blood endothelial cells were seen at the core and edge of the organoids as marked by CD31 staining. LYVE1 staining in the periphery of the organoids also demonstrated the presence of lymphatic endothelial cells (Fig 1C). To confirm that the different cells were present in the organoid, we performed western blot analyses, which showed markers for epithelial cells (E-Cadherin), fibroblasts (vimentin), HUVEC cells (CD31) and lymphatic endothelial cells (LYVE1) (Fig 1D).

Scanning electron microscopic (SEM) analyses of the PLiD reveals an uneven surface architecture with irregular bulging segments, which are typical of surface epithelial cells in the lung (Fig. 1E) (11,12). Transmission electron microscopy (TEM) micrographs of ultrathin organoid sections at 800X magnification show a number of projections including surface blebs and short microvilli, which are protruding into the luminal spaces (Fig. 1F). TEM images also show unusual cytoplasmic features with the presence of numerous multilamellar bodies with parallel membranes (Fig 1G). Pulmonary lamellar bodies store surfactant proteins (SP) that are processed in the rough endoplasmic reticulum and the golgi apparatus (13). Some of the lamellar bodies contain small vesicles. These organelles are implicated in the secretion of SP that spread over the alveolar surfaces providing an extracellular coating. Pulmonary SP secreted by epithelial cells consists of phospholipids, glycosaminoglycans and proteins that together reduce the surface tension allowing the exchange of gases and material during inspiration (14).

As mentioned above, lamellar bodies produced by the epithelial cells in the lung store multiple surfactant proteins (SP), of which SP-B and SP-C are essential for lowering the surface tension at the air/liquid interface within the alveoli of the lung (15). As a surrogate for lung function, we determined SP expression. Western blotting of PLiD lysates demonstrated the presence of SP-B and SP-D, which were at higher levels in the PLiD organoids than 2D cultures of NL20 cells, further demonstrating that the PLiD organoid is functionally similar to the human lung (Fig 1H).

Previous studies have demonstrated that PBMCs can infiltrate 3D cultures of human non-small cell lung cancer (NSCLC) cell lines, grown alone or with a human fibroblast cell line (16). To determine if the PLiD cultures are amenable to PBMC infiltration, we labeled PBMCs with PKH26 dye and then added them to PLiD cultures. Immunofluorescence image, taken after 3 days shows that the labeled cells are within the lung organoid ((Supplementary Fig S1C, top panel). To determine the depths to which the cells have penetrates, we took images at 50 μM intervals shows penetration of PBMC's through the entirety of the PLiD spheroids (Supplementary Fig S1C, bottom panel).

Metastatic Tumor-In-A-Dish is an effective platform for studying cancer cell colonization

Currently, no models are available to efficiently study lung colonization of metastatic cells. The only available method to study lung colonization is an animal model, where cancer cells are injected into the tail vein and subsequent growth in the lungs is measured. Although more reliable, animal experiments are expensive and don't take into consideration the complexity of multiple human cell types interacting in a concerted manner with the tumor

(17). To circumvent this critical issue, we developed a metastatic tumor-in-a-dish (mTiD) model that recreates the tumor microenvironment and allows for medium to high throughput screening of therapeutic agents (Supplementary Fig S1D). We seeded colon carcinoma cells along with the PLiD cells in non-adherent dishes to generate mTiD organoids. Histological examination of the mTiD organoids looks similar to that of colon cancer metastasis to the lung (Fig 2A). Focal central necrosis is a common feature of tumors with blood supply that is primarily on the periphery of the tumor (18). We observed central necrosis in the mTiD cultures from 2 colon cancer cell lines due to a hypoxic core as assessed by hypoxia tracer hypoxyprobe-Red549 (Fig 2B). To further confirm that the endothelial cells are present in the mTiD, we generated the tumor organoids using fluorescently labeled endothelial cells, along with 3 colon carcinoma cell lines. An even distribution of GFP labeled colon carcinoma cells were observed throughout the organoid (Fig 2C). In discrete regions interspersed between the carcinoma cells were vessel-like tubule structures of mCherry (red) labeled endothelial cells. Organoids were dissociated and single cell suspensions were assessed by flow cytometry to determine the percentage of carcinoma and endothelial cells in the organoids. We found that close to 50% of the organoid consisted of carcinoma cells and 9–11% of endothelial cells (Fig 2D). Western blotting analyses revealed that all the cell types seeded were represented within the organoids and expressed the individual markers, namely E-cadherin for epithelial cells, vimentin for fibroblasts, CD31 and LYVE1 for blood and lymph endothelial cells respectively and SPB and SPD for lung epithelial cells (Fig 2E).

We next determined if the cancer cells can colonize PLiD, for which we first allowed PLiD to develop, and subsequently added GFP-labeled HCT116 cancer cells. We obtained images at various time point after addition of the GFP-labeled cells in PLiD culture. At 12 h, we observed one cell to be attached to the PLiD, which formed a small colony after 3 days and after and grew to be a larger GFP positive HCT116 colony after 5 days (Fig 3A). Since angiogenesis is important for tumor growth, we next determined the effect of the cancer cell colonization in the lung organoid on blood vessel formation. Immunohistochemical staining of sections from the mTID shows a single CD31 positive blood vessel like structure in the center of PLiD and some positive staining in periphery. However, in the mTiD, there were multiple branches of CD31 positive cells, suggesting that the cancer cells enhanced the angiogenic process in the mTiD model organoid (Fig 3B).

Exosomes are small membrane-bound vesicles that carry various cargo including nucleic acids such as DNA, mRNA, miRNA, and proteins. Exosomes are involved in intercellular signaling and EMT, resulting in cancer cells presenting a more aggressive phenotype (19–21). Recent studies have demonstrated that exosomes isolated from highly metastatic murine breast cancer cells distributed predominantly to the lung, and enhanced breast cancer cell metastases (22). To determine whether cancer cell colonization of PLiD is affected by exosomes, we pretreated PLiD with exosomes secreted by HCT116 colon cancer cells grown in 2D culture. Subsequently, we added HCT116 cells to the PLiD and allowed the cells to colonize for 3 days. We observed significantly bigger and higher number of colonization following exosome treatment suggesting that the exosome sufficiently modulate the lung to enhance the colonization process (Fig 3C).

Metastatic Tumor-In-A-Dish is an effective platform for determining sensitivity to therapeutic agents

Current *in vitro* screening methods are poorly predictive of the clinical efficacy of drug candidates. Also, as mentioned above, animal experiments are expensive and not appropriate to study human cancer cell response to therapeutics. It is also well known that the stromal cells modulate the response of tumor cells to therapeutic agents (23). We therefore determined whether the mTiD model would be efficient for studying therapeutic response of cancer cells. First, we tested the effect of the anti-VEGF antibody Bevacizumab because VEGF plays an important role in tumor growth and metastasis (24,25). Moreover, targeting VEGF was considered to be good therapeutic option for patients with metastatic colorectal cancer, especially in combination with current therapeutic agents (26,27). We treated the mTiD model containing GFP-labeled colon cancer cells DLD1 and SW480 with increasing concentrations of Bevacizumab. There was a dose dependent decrease in GFP labeled cells in mTiD upon treatment (Fig 4). This suggests that the model is amenable to testing biological agents which may include immune therapy agents.

Since patients are administered various combinations of agents including 5-fluouracil (5FU), oxaliplatin, irinotecan and leucovorin, we tested the antitumor efficacy of these compounds in the mTID model. We observed significant inhibition in growth of the three colon cancer cell lines HCT116, SW480 and DLD1 when treated with either irinotecan or SN38, an active metabolite of irinotecan (Fig 5A, Supplementary Table S2A).

The most striking observation was that HCT116 cells did not respond to 5FU while DLD1 cells did not respond to oxaliplatin in the mTiD model, with IC50s >25 μM (Fig 5A). However, in 2D single cell type cultures, 5FU suppressed HCT116 cell growth with IC50 of 13.2 ± 2.08 μM, and oxaliplatin suppressed DLD-1 cells with an IC50 of 7.4 μM ± 3.05 (Fig 5B, Supplementary Table S2B). We also performed studies on single cell type 3D cultures of HCT116 (Fig 5C), SW480 (Fig 5D) and DLD1 (Fig 5E). Interestingly, the 3D cultures were not susceptible at these doses. Much higher dose of compounds was required to observe some effect in the 3D single cell type cultures. In addition, irinotecan did not affect the cells in the 3D cultures, although its active metabolite SN38 showed significant efficacy. This suggests that the poor response to irinotecan in 3D single cell type cultures may be due to poor metabolism of the drug to its active component. These data further suggest that the mTiD model is the most appropriate model for testing drugs because it is a better representative of tumor physiology than the 3D single cell type spheroids.

To determine whether PLiD cultures has utility for assessing toxicity of therapeutics to the lung, we evaluated the dose response of PLiD cultures to increasing concentrations of 5FU, cisplatin, carboplatin, oxaliplatin, irinotecan and SN38. PLiD cultures demonstrated reduced spheroid sizes or dispersed spheroids only at very high concentrations of these compounds suggesting that the drugs are not directly affecting the cultures at pharmacological doses (Supplementary Fig S2).

In order to further assess the effectiveness of the mTiD platform in other tumor types, we also performed extensive testing of ovarian cancer cell lines. We grew A2780 human ovarian cancer cell line and its cisplatin resistant variant C30 in 2D and mTiD cultures. Both cells

were efficiently taken up in the mTiD cultures (Fig 5F). We next determined the effect of 5FU, cisplatin, oxaliplatin and carboplatin in 2D and mTiD cultures. Specifically, we saw a striking difference in drug response in the mTiD cultures compared to 2D cultures. While the parent A2780 cells showed IC50 values between 24.6 and 53.2 μM, the C30 cells had IC50 values of >100 μM in mTiD cultures (Fig 5G. Supplementary Table S2C). However, both the parent A2870 and its C30 derivative demonstrated lower IC50 values in 2D cultures (Fig 5H, Supplementary Table S2D). These data again confirm that the responses to drug treatment in the mTiD model, but not 2D or 3D cultures replicates what is observed in humans.

Finally, we tested the ability of additional cancer cell types including glioblastoma (U251), medulloblastoma (DAOY), and breast cancer (MCF7) to form mTiD cultures (Supplementary Fig S3A-C). In addition, we tested the response of the mTID cultures to 5FU because it is a standard of therapy for these diseases. While glioblastoma cells in the mTiD are responsive to 5FU, medulloblastoma and breast cancer cells in the mTiD cultures were resistant (Supplementary Fig S3A-C). We also tested these cancer cells in the mTiD with honokiol, a natural compound found in the bark of the magnolia tree. All the cultures were sensitive to the compound. Finally, melanoma cells are known to frequently metastasize to the lung. Moreover, patients who are treated with vemurafenib, the first line treatment for this indication develop resistance. We tested the response of paired vemurafenib sensitive and resistant A2058 melanoma cells to honokiol. We observed that honokiol treatment effectively reduced growth of both vemurafenib sensitive and resistant cells (Supplementary Fig S3D).

Metastatic Tumor-In-A-Dish is amenable to study metastasis prevention

Developing potential strategies for preventing tumor metastasis has been somewhat difficult study in part due to lack of adequate models of disease. Currently, the only methods to study would be using mouse models, but this model may not work for every cancer type because of lack of disease models for metastatic research. A second point to consider is whether the cancer cells that have disseminated from the primary tumor site able to colonize and grow in the metastatic site. Given that the mTiD model is designed to study colonization and growth of disseminated cells, we performed two different experiments that would replicate a prevention setting. In the first experiment, we treated PLiD with chemotherapeutic agents (5FU, Irinotecan and Oxaliplatin) at IC50 values for 24 h and then added mCherry-labeled cancer cells (Supplementary Fig S4A). We observed significantly lower numbers of cancer cells colonizing the PLiD in the treated samples when compared to controls suggesting that pretreatment of PLiD can suppress tumor cell colonization. In a second experiment, we first treated mCherry-expressing cancer cells with the drugs at the IC50 dose for 24 h and then added these cells to the PLiD (Supplementary Fig S4B). Again, there was significantly lower number of cancer cells colonizing the PLiD, suggesting that drug treatment suppresses colonization. Taken together, these data suggest that the mTiD system would be an effective method to determine mechanisms to prevent cancer cell colonization.

mTiD is an effective platform to screen for drug sensitivity in primary cancer cells

Currently, there are no standard chemotherapeutic agents for metastatic colon cancer. As mentioned above, patients are administered combinations of several agents. Also, there are no tests or biomarkers that can effectively predict the sensitivity of patients to the various chemotherapeutic agents. We used the mTiD platform to test the efficacy of various chemotherapeutic agents in 2 primary colon carcinoma lines (hCol1 and hCol2). The patient characteristics are listed in Supplementary Table S1. We used whole genome exome sequencing on hCol2 primary tumor and matched cells in culture to determine the genomic variance. Available paraffin embedded tissue samples from hCOL1 did not yield the necessary quality of RNA for sequencing analyses. Despite cellular heterogeneity, the primary tumor had 64.96% homology in the mutation profile compared to the matched colon cancer cells growing in culture, demonstrating that the primary cells are similar to the patient samples (Supplementary Fig S5 and Supplementary Table S3). Again, the GFP-labeled patient derived primary cells were able to colonize the lung and form metastatic tumors (Fig 6A). We then tested the antitumor efficacy of 5FU, irinotecan, oxaliplatin and SN38 in the primary patient derived mTiD cultures. In these cultures, both hCol1 and hCol2 were resistant to oxaliplatin with IC50s >25 μM (Fig 6B and Supplementary Table S4). In addition, the hCol1 mTiDs were resistant to 5FU and irinotecan. The hCol2 mTiD was sensitive to irinotecan with an IC50 of 0.3 ± 0.07 μM. Both hCol1 and hCol2 were sensitive to SN38 with IC50 values of 0.45 ± 0.19 μM and 0.075 ± 0.01 μM, respectively. In 2D cultures, both hCol1 and hCol2 were sensitive to all the agents with IC50 values ranging from 0.05 ± 0.01 μM – 9 ± 1.12 μM (Supplementary Table S4 and Supplementary Fig S6A). Moreover, when cancer cells were grown as single cell type 3D spheroids, we needed much higher concentrations of drug than what was required for 2D or mTiD cultures, further suggesting that this method of growing and testing culture is not appropriate (Supplementary Fig S6B).

To validate the sensitivity of the mTiD cultures to chemotherapeutic agents, we assessed the levels of carcinoembryonic antigen (CEA) in the cell lysates and supernatants of primary hCol mTiD cultures. The hCol2 mTiD cells were sensitive to 5FU, irinotecan and SN38 and demonstrated a corresponding reduction in CEA levels in both the cell lysates and supernatant (Fig 6C,D). Further, hCol2 mTiD cells demonstrated oxaliplatin resistance, and a corresponding lack of change in CEA levels in both the cell lysate and supernatant. To further validate these findings, we used the chemiluminescent immunoassay (CLIA) to measure the levels of CEA in cell supernatants. Corroborating our cell viability data, hCol1 cells that were sensitive to only SN38, showed a corresponding 50% reduction in CEA levels with SN38 treatment but a 35–40% reduction in CEA levels on treatment with 5FU, irinotecan and oxaliplatin, respectively (Fig 6E). Similarly, hCol2 cells showed >60% reduction in CEA levels on 5FU, irinotecan and SN38 treatment but only 20% reduction in CEA levels when treated with oxaliplatin.

To further confirm that the mTiD model recapitulated the patient’s response to therapy, we interrogated serum from the patient whose tumor was used to derive the hCol2 line. The hCol1 patient was not treated with chemotherapy because of severe toxicity. The hCol2 patient was treated with a combination of avastin, FOLFIRI (irinotecan, 5FU and

leucovorin), capecitabine and oxaliplatin. Serum levels of CEA went down from 100 to 3 ng/ml post chemotherapy and stayed low even 200 d post-surgery (Fig 6F). This finding is consistent with the data from the mTiD platform, which effectively demonstrated the sensitivity of the patient to FOLFIRI as determined by the cell survival and CEA levels. Thus, mTiD may be an effective platform to predict the sensitivity of patients undergoing colon cancer chemotherapy.

mTiD is an effective platform to screen for drug sensitivity in primary ovarian cancer cells

To further assess the effectiveness of the mTiD platform in other a second tumor type, we tested ovarian cancer cell lines and primary ovarian cancer cells from ascitic fluid that has a propensity to metastasize to the lung. For this, we isolated ovarian cancer cells from ascites fluid of two patients with ovarian cancer (hOVR1 and hOVR2). The patient characteristics are listed in Supplementary Table S1. As above with colon cancers, we performed whole genome exome sequencing on hOVR1 ascites fluid and matched cells in culture. Despite cellular heterogeneity, analyses of mutation profiles showed 98.41% homology between DNA isolated from the ascites fluid and the matched cancer cells growing in culture (Supplementary Fig S5 and Supplementary Table S3). We first tested two primary ovarian carcinoma cells for growth in PLiD. Our data demonstrate that GFP-labeled primary metastatic ovarian cancer cells grow well in the mTiD model with distribution throughout the organoid (Fig 7A). Further, flow cytometry analyses revealed that organoids contained 25–27% GFP-labeled tumor cells. We next checked the sensitivity of 2D- and mTiD-hOVR1 and hOVR2 cultures to 5FU, irinotecan, oxaliplatin, cisplatin and carboplatin. In 2D cultures, hOVR1 and hOVR2 cells were sensitive to 5FU, oxaliplatin, irinotecan and cisplatin with IC50 values ranging from 1–18 μM (Supplementary Fig S7A and Supplementary Table S5). Again, similar to that seen with colon cancer cells above, when cells were grown as single cell type 3D spheroids, the levels of drug required for cytotoxicity was much higher than what was observed in 2D cultures, ranging from 15– 212.5 μM (Supplementary Fig S7B,C). In mTiD cultures, hOVR1 was sensitive to 5FU, irinotecan, oxaliplatin and cisplatin with IC50 values of 10, 4, 4.25 and 10.25 μM, respectively (Fig 7B and Supplementary Table S5). In mTiD cultures, hOVR2 was sensitive to 5FU and irinotecan at IC50 values of 10 and 4 μM, respectively. However, hOVR2 cells were resistant to oxaliplatin (IC50 > 25 μM) and cisplatin (IC50 >25 μM).

Primary ovarian cancer mTiD cultures accurately reflect patient response to carboplatin

The current choice of first-line chemotherapy in ovarian cancer patients is not based on rational design. The ability to predict response of patients to specific chemotherapeutics would facilitate the rapid and effective treatment of cancer patients. Generally, the patients receive cisplatin or carboplatin, and they generally appear to respond to the drug. However, a majority of the cases have reemergence of the tumor, and these are now resistant to the platin drugs. In our studies hOVR1 is from a patient that had never been treated with platin drugs (carboplatin naive), while hOVR2 is from a patient that is resistant to carboplatin. To confirm that our OVR mTiD cultures replicates this, we tested them for sensitivity to carboplatin. Our data demonstrate that hOVR1 was sensitive to carboplatin at an IC50 value of 30 μM while hOVR2 was resistant with an IC50 value of >25 μM (Fig 7C). We assessed for secreted CA125 levels from the two OVR mTiD cultures. The data demonstrates that

carboplatin treatment of the naïve patient-derived hOVR1 culture had a corresponding 80% reduction in secreted CA125 levels when treated with various concentrations of carboplatin (Fig 7D). The hOVR2 cultures on the other hand, demonstrated resistance to carboplatin in the mTiD cultures with a reduction in CA125 levels by only 30% at the highest carboplatin dose of 25 μM. In order to determine the clinical relevance of these *in vitro* findings, we obtained the data from the clinical laboratory on CA125 levels in patient's serum beginning on the day of surgery (Day 0) for up to 300 days. The hOVR1 patient was treated with taxol, cisplatin and doxorubicin and demonstrated a reduction in CA125 levels with levels below 35 U/ml (Fig 7E). The hOVR2 patient in contrast, demonstrated an initial drop in CA125 levels post-surgery that were reduced 100 d post-surgery. The patient was administered a combination of taxol and carboplatin as first-line therapy. CA125 levels went up in the patient serum following relapse of the tumor, which was corroborated by the hOVR2-mTiD *in vitro* data (Fig 7F).

Discussion

While primary neoplasms generally have a favorable prognosis, metastatic spread is the major cause of cancer-related mortality, for which there are few therapeutic options. A major hurdle in the development of anti-metastatic therapies is the dearth in effective preclinical models to study and to develop targeted therapies that prevent or treat metastatic disease. To date, 2D assays were the main stay for drug screening, in part because they can be easily observed and growth measured. However, it has become increasingly apparent that this method lacks the *in vivo* characteristics seen in a tumor. Rigid surfaces used in 2D culture enhance proliferation but likely inhibit differentiation due to lack of cell-cell interactions (28,29). In addition, these rigid surfaces result in flattened cell growth and changes in the cytoskeleton, which then changes nuclear shape, which has been shown to cause differences in gene expression and protein synthesis (30). Finally, previous studies corroborate our data demonstrating that tumor cell lines in 2D cultures may be more susceptible to therapeutic agents when compared to cells grown as 3D spheroids (31–33). However, the single cancer cell type 3D spheroids do not replicate the *in vivo* setting as they only employ cancer cells and do not have stromal cells. Moreover, 3D cultures of just the cancer cells require significantly higher levels of drug to see effects, and this is not representative of what happens in the *in vivo* setting. Another pitfall of current 3D tumor models is that they are created with commercially available cell cultures that no longer reflect the pathology and chemoresistance patterns that are seen *in vivo*. It is also becoming increasingly apparent that the tumor microenvironment pays a significant role in cancer progression and response to therapy (34,35). Although tumor cells alter the microenvironment to support their growth and metastasis (36–38), little is known about the tumor-associated stromal cells. The major hurdle in carrying out these studies has been the acquisition and establishment of primary stromal cells from patient samples.

In recent years, there has been a surge in technologies wherein cells can be cultured in ways that maintain their natural morphology and structure. It is for this reason that 3D cell culturing such as tumor organoids were developed, resulting in enhanced physiological relevance of experiments performed *in vitro*. Because there is more cell-to-cell contact, and in return more intercellular signaling, cells develop more complex structures. This cell

culture environment could improve the predictive accuracy of the drug discovery process and aid in the understanding of tissue morphogenesis (39,40). Thus, while 2D culture is reproducible, it is a highly artificial and less physiological environment, as some *in vivo* characteristics and traits are lost or compromised. In contrast, 3D cell culture is more physiological with these traits better preserved (1).

The choice of the appropriate organoid model and culturing conditions is a crucial decision in the design of experiment with these 3D cultures, as each has advantages and disadvantages. Currently 3D tumor models can essentially be divided into scaffold-based and scaffold- free models (41). Scaffold-based 3D models are numerous and varied and can incorporate both natural and synthetic materials including collagen, fibrin, Hyaluronic acid, silk, and alginate (42–45). These materials are easier to reliably reproduce but are not always physiologically relevant. Studies have also tried using cancer fibroblast associated matrices, which may be more accurate in resembling the tumor microenvironment as compared to artificial scaffolds; however, these too do not recapitulate the tumor microenvironment in a metastatic setting (46). Another issue is that even with fibroblast-derived matrices, the cultures do not represent the metastatic tumor in the lung (47).

In general, scaffold-free systems may better represent human lung metastatic tumor, wherein the cells form their own extracellular matrix. However, in most cases, only single cell type 3D spheroids have been studied. Nevertheless, these methods have provided us invaluable insights into cancer stem cell biology and differentiation as well as modeling tumor hypoxia, given that the innermost cells have limited oxygen exposure (48). Tumor organoids are well established in basic cancer research and experimental therapeutics, and have shown resistance to chemotherapy-induced apoptosis when compared to identical cells in monolayers (3). But it is clear that the versatility of organoids offers an advantage over other models to further understand cancer biology.

In our study we have developed a new *in vitro* lung organoid, PLiD, which contains all the normal lung cells including epithelial cells, fibroblast and endothelial cells. The data establishes expression of E-cadherin (epithelial cells), vimentin (fibroblast), CD31 (Heme-Endothelial cells) and LYVE1 (lymphatic endothelial cells) in PLiD using immunocytochemistry indicating the presence of multiple viable cell types in the organoid. Furthermore, this PLiD model demonstrates significant expression of surfactant proteins (B and D), an indication of functional lung tissue. Expression of surfactant protein was seen only in PLiD model, and not in cells grown individually. Our studies further confirm that PLiD cultures may be an excellent platform to study the final process of metastasis namely colonization. Current *in vitro* methods to study colonization use artificial matrices or bioengineered 3D platforms (49,50). However, while many such matrices may be useful to study cancer cell growth and migration (51), they have not been amenable to study angiogenesis. In the PLiD system, we have observed angiogenesis after colonization by the cancer cells. We planned to test both HUVEC and HLMVEC in our model. Initially, we tried both types of cells but the HMVEC cells failed to thrive in the PLiD model, which is a limitation. However, HUVEC cells worked really well in the model. Given that these cells are robust lines to study growth and tube forming ability, and they thrived in the model we carried out all studies with this line. In addition to developing studies to understand the role

of angiogenesis in cancer cell colonization, the system may be useful in learning about the mechanisms by which cancer cells induce the angiogenic process. In addition, given that pretreatment of PLiD with cancer cell derived exosomes enhanced cancer cell colonization, further underscores the role of this model to study the effect of circulating factors and those in the microenvironment cancer cell colonization.

Another utility for PLiD/mTiD is in drug development and assessing toxicity. While all our current studies are performed with cells in traditional 2D and more recent 3D multicellular spheroid systems that may include fibroblasts, none of them replicate the organ in the body. Hence, after the preliminary cell culture work, one has to rely on studies in animals such as mice. There are two problems with this approach, the expenditure involved in maintaining the animals and a second, more ethical dilemma of having to use animals for the such discovery studies because of issues such as distress. Moreover, animal tissues do not always replicate what is seen in the humans. With the development of the PLiD/mTiD system, we now have an effective platform to assess the ability of primary tumor and established cell lines to colonize the lung and further assess response to chemotherapy. Moreover, for those in the drug development field, this system would be an excellent intermediate between current 2D and 3D cultures and animal studies. The system can also be used to determine the role of immune cells in therapeutic responses. Finally, not only can the new compounds and biological agents be tested against various mTID models (developed with different cancer cells), but also on PLiD to determine issues related to toxicity. Adverse drug reactions are a common form of injury and the lungs are a frequent target. However, current toxicity testing involves cell lines in traditional 2D cultures or in a chip (52). However, none of these replicate the organ. Hence, given the lung architecture seen in PLiD, it may be an excellent model to study drug-related toxicity. In this regard, all our studies presented in this manuscript with the various drugs also included testing the compounds in PLiD to ensure that the dose of drug used to kill the cancer cells in mTiD was not also affecting the lung cells in PLiD. Finally, the possibility exists that the model can be used to study other lung-related diseases such as cystic fibrosis and infections.

The aim of precision medicine is to identify patients with tumors that are most likely to respond to specific chemotherapeutic agents. We and others have demonstrated that the response of primary tumor cells to chemotherapy varies in 2D versus 3D cultures (53). However, no one has been able to correlate this to patient response to the chemotherapeutic agent. One of the strengths of our study is that we have successfully cultured primary patient-derived cells *ex vivo* in the mTiD system, and the responses to the clinically relevant therapeutics observed in the mTiD organoids closely resembled that seen in the patients. However, while this is the first presentation of the model, we did not have access to metastatic lung tumors to compare with the mTiD model, because patients with metastatic disease are not surgically treated. Nevertheless, further studies are warranted to demonstrate that PLiD/mTiD model represents the in vivo patient tumor and its microenvironment in terms of genetic characteristics, which is a future direction of our studies A matched primary analysis, such as global gene expression patterns or genomic mutations would be valuable for comparing individual profiles but would inherently select for a subgroup of cancer cells and may not provide sufficient information about modeling intra-tumoral heterogeneity.

Our data suggest that the response of mTiD cultures from primary tumors may correlate with that of patients to chemotherapy. One of the limitations of our study is the sample size, and hence may not account for differences in therapeutic response of individual patient tumors. Hence, further studies with a large cohort of patient samples are required to confirm our findings. Another factor relates to intra-tumoral heterogeneity, something that has not been tested at this time in this mTiD model. It should be noted that not all tumors have intra-tumoral heterogeneity (54). Nevertheless, future studies are required with tumors known to have intra-tumoral heterogeneity and compare therapeutic response in the mTiD model to single cell type 3D cultures.

Patient-derived xenografts are being employed for drug screening (55). However, implanted tumors in mice need to be expanded into multiple mice prior to drug screening for sensitivity. This process is time consuming, cumbersome and costly. Moreover, the xenografts have significant infiltration of mouse cells further complicating understanding of the results. On the other hand, the mTiD model effectively overcomes these limitations in that, the cells are in 3D in the context of the human lung microenvironment, thereby allowing for the screening of drugs that would effectively target lung metastatic disease. Thus, the mTiD platform can be used as a tool to inform decision pertaining to the selection of appropriate chemotherapeutic agents for individual patients depending on their drug sensitivity profile.

Supplementary Material

Refer to Web version on PubMed Central for supplementary material.

Acknowledgements:

Funding:

This work was supported by the NIH grants CA135559 and CA109269, the Kansas Bioscience Authority, Tom O'Sullivan Foundation Supported Research and grants from the Braden's Hope Foundation and Midwest Cancer Alliance. We would also like to acknowledge the support of the National Cancer Institute Cancer Center Support Grant P30CA168524, which supports the Biospecimen Repository Shared Resource that provided the deidentified patient samples. We thank the University of Kansas Medical Center – Genomics Core for generating the sequence data sets. The Genomics Core is supported by the University of Kansas School of Medicine, the Kansas Intellectual and Developmental Disability Research Center (NIH U54 HD090216) and the Molecular Regulation of Cell Development and Differentiation - COBRE (5P30GM122731–02).

References:

1. Miller KD, Siegel RL, Lin CC, Mariotto AB, Kramer JL, Rowland JH, et al. Cancer treatment and survivorship statistics, 2016. CA Cancer J Clin 2016;66:271–89 [PubMed: 27253694]
2. Klinghammer K, Walther W, Hoffmann J. Choosing wisely - Preclinical test models in the era of precision medicine. Cancer Treat Rev 2017;55:36–45 [PubMed: 28314175]
3. Lovitt CJ, Shelper TB, Avery VM. Advanced cell culture techniques for cancer drug discovery. Biology (Basel) 2014;3:345–67 [PubMed: 24887773]
4. Xu X, Farach-Carson MC, Jia X. Three-dimensional in vitro tumor models for cancer research and drug evaluation. Biotechnol Adv 2014;32:1256–68 [PubMed: 25116894]
5. Bielecka ZF, Maliszewska-Olejniczak K, Safir IJ, Szczylik C, Czarnecka AM. Three-dimensional cell culture model utilization in cancer stem cell research. Biol Rev Camb Philos Soc 2017;92:1505–20 [PubMed: 27545872]

6. Tario JD, Jr., Muirhead KA, Pan D, Munson ME, Wallace PK Tracking immune cell proliferation and cytotoxic potential using flow cytometry. Methods Mol Biol 2011;699:119–64 [PubMed: 21116982]
7. Xu R, Greening DW, Rai A, Ji H, Simpson RJ. Highly-purified exosomes and shed microvesicles isolated from the human colon cancer cell line LIM1863 by sequential centrifugal ultrafiltration are biochemically and functionally distinct. Methods 2015;87:11–25 [PubMed: 25890246]
8. Kaushik G, Venugopal A, Ramamoorthy P, Standing D, Subramaniam D, Umar S, et al. Honokiol inhibits melanoma stem cells by targeting notch signaling. Mol Carcinog 2015;54:1710–21 [PubMed: 25491779]
9. Budczies J, von Winterfeld M, Klauschen F, Bockmayr M, Lennerz JK, Denkert C, et al. The landscape of metastatic progression patterns across major human cancers. Oncotarget 2015;6:570–83 [PubMed: 25402435]
10. Heaton TE, Davidoff AM. Surgical treatment of pulmonary metastases in pediatric solid tumors. Semin Pediatr Surg 2016;25:311–7 [PubMed: 27955735]
11. Bachofen H, Schurch S. Alveolar surface forces and lung architecture. Comp Biochem Physiol A Mol Integr Physiol 2001;129:183–93 [PubMed: 11369543]
12. Mercer BA, Lemaitre V, Powell CA, D'Armiento J. The Epithelial Cell in Lung Health and Emphysema Pathogenesis. Curr Respir Med Rev 2006;2:101–42 [PubMed: 19662102]
13. Perez-Gil J Structure of pulmonary surfactant membranes and films: the role of proteins and lipid-protein interactions. Biochim Biophys Acta 2008;1778:1676–95 [PubMed: 18515069]
14. Serrano AG, Perez-Gil J. Protein-lipid interactions and surface activity in the pulmonary surfactant system. Chem Phys Lipids 2006;141:105–18 [PubMed: 16600200]
15. Veldhuizen EJ, Haagsman HP. Role of pulmonary surfactant components in surface film formation and dynamics. Biochim Biophys Acta 2000;1467:255–70 [PubMed: 11030586]
16. Koeck S, Kern J, Zwierzina M, Gamerith G, Lorenz E, Sopper S, et al. The influence of stromal cells and tumor-microenvironment-derived cytokines and chemokines on CD3(+)CD8(+) tumor infiltrating lymphocyte subpopulations. Oncoimmunology 2017;6:e1323617 [PubMed: 28680763]
17. Jackson SJ, Thomas GJ. Human tissue models in cancer research: looking beyond the mouse. Dis Model Mech 2017;10:939–42 [PubMed: 28768734]
18. Caruso RA, Branca G, Fedele F, Irato E, Finocchiaro G, Parisi A, et al. Mechanisms of coagulative necrosis in malignant epithelial tumors (Review). Oncol Lett 2014;8:1397–402 [PubMed: 25202341]
19. Bigagli E, Luceri C, Guasti D, Cinci L. Exosomes secreted from human colon cancer cells influence the adhesion of neighboring metastatic cells: Role of microRNA-210. Cancer Biol Ther 2016:1–8
20. Vella LJ. The emerging role of exosomes in epithelial-mesenchymal-transition in cancer. Front Oncol 2014;4:361 [PubMed: 25566500]
21. Lugini L, Valtieri M, Federici C, Cecchetti S, Meschini S, Condello M, et al. Exosomes from human colorectal cancer induce a tumor-like behavior in colonic mesenchymal stromal cells. Oncotarget 2016;7:50086–98 [PubMed: 27418137]
22. Wen SW, Sceneay J, Lima LG, Wong CS, Becker M, Krumeich S, et al. The Biodistribution and Immune Suppressive Effects of Breast Cancer-Derived Exosomes. Cancer Res 2016;76:6816–27 [PubMed: 27760789]
23. Shi Y, Du L, Lin L, Wang Y. Tumour-associated mesenchymal stem/stromal cells: emerging therapeutic targets. Nat Rev Drug Discov 2017;16:35–52 [PubMed: 27811929]
24. Zhang L, Hannay JA, Liu J, Das P, Zhan M, Nguyen T, et al. Vascular endothelial growth factor overexpression by soft tissue sarcoma cells: implications for tumor growth, metastasis, and chemoresistance. Cancer Res 2006;66:8770–8 [PubMed: 16951193]
25. Verheul HM, Hammers H, van Erp K, Wei Y, Sanni T, Salumbides B, et al. Vascular endothelial growth factor trap blocks tumor growth, metastasis formation, and vascular leakage in an orthotopic murine renal cell cancer model. Clin Cancer Res 2007;13:4201–8 [PubMed: 17634549]
26. Collins TS, Hurwitz HI. Targeting vascular endothelial growth factor and angiogenesis for the treatment of colorectal cancer. Semin Oncol 2005;32:61–8 [PubMed: 15726507]

27. Grapsa D, Syrigos K, Saif MW. Bevacizumab in combination with fluoropyrimidine-irinotecan- or fluoropyrimidine-oxaliplatin-based chemotherapy for first-line and maintenance treatment of metastatic colorectal cancer. Expert Rev Anticancer Ther 2015;15:1267–81 [PubMed: 26506906]
28. Pampaloni F, Reynaud EG, Stelzer EH. The third dimension bridges the gap between cell culture and live tissue. Nat Rev Mol Cell Biol 2007;8:839–45 [PubMed: 17684528]
29. Elliott NT, Yuan F. A review of three-dimensional in vitro tissue models for drug discovery and transport studies. J Pharm Sci 2011;100:59–74 [PubMed: 20533556]
30. Birgersdotter A, Sandberg R, Ernberg I. Gene expression perturbation in vitro--a growing case for three-dimensional (3D) culture systems. Semin Cancer Biol 2005;15:405–12 [PubMed: 16055341]
31. Edmondson R, Broglie JJ, Adcock AF, Yang L. Three-dimensional cell culture systems and their applications in drug discovery and cell-based biosensors. Assay Drug Dev Technol 2014;12:207–18 [PubMed: 24831787]
32. Ravi M Applications of Three-Dimensional Cell Cultures in the Early Stages of Drug Discovery, Focusing on Gene Expressions, Drug Metabolism, and Susceptibility. Crit Rev Eukaryot Gene Expr 2017;27:53–62 [PubMed: 28436332]
33. Levinger I, Ventura Y, Vago R. Life is three dimensional-as in vitro cancer cultures should be. Adv Cancer Res 2014;121:383–414 [PubMed: 24889536]
34. Albini A, Sporn MB. The tumour microenvironment as a target for chemoprevention. Nat Rev Cancer 2007;7:139–47 [PubMed: 17218951]
35. Correia AL, Bissell MJ. The tumor microenvironment is a dominant force in multidrug resistance. Drug Resist Updat 2012;15:39–49 [PubMed: 22335920]
36. Whiteside TL. The tumor microenvironment and its role in promoting tumor growth. Oncogene 2008;27:5904–12 [PubMed: 18836471]
37. Ungefroren H, Sebens S, Seidl D, Lehnert H, Hass R. Interaction of tumor cells with the microenvironment. Cell Commun Signal 2011;9:18 [PubMed: 21914164]
38. Chang CH, Qiu J, O'Sullivan D, Buck MD, Noguchi T, Curtis JD, et al. Metabolic Competition in the Tumor Microenvironment Is a Driver of Cancer Progression. Cell 2015;162:1229–41 [PubMed: 26321679]
39. Knight E, Przyborski S. Advances in 3D cell culture technologies enabling tissue-like structures to be created in vitro. J Anat 2015;227:746–56 [PubMed: 25411113]
40. Maltman DJ, Przyborski SA. Developments in three-dimensional cell culture technology aimed at improving the accuracy of in vitro analyses. Biochem Soc Trans 2010;38:1072–5 [PubMed: 20659006]
41. Weiswald LB, Bellet D, Dangles-Marie V. Spherical cancer models in tumor biology. Neoplasia 2015;17:1–15 [PubMed: 25622895]
42. Willerth SM, Arendas KJ, Gottlieb DI, Sakiyama-Elbert SE. Optimization of fibrin scaffolds for differentiation of murine embryonic stem cells into neural lineage cells. Biomaterials 2006;27:5990–6003 [PubMed: 16919326]
43. Mauney JR, Nguyen T, Gillen K, Kirker-Head C, Gimble JM, Kaplan DL. Engineering adipose-like tissue in vitro and in vivo utilizing human bone marrow and adipose-derived mesenchymal stem cells with silk fibroin 3D scaffolds. Biomaterials 2007;28:5280–90 [PubMed: 17765303]
44. Gerecht S, Burdick JA, Ferreira LS, Townsend SA, Langer R, Vunjak-Novakovic G. Hyaluronic acid hydrogel for controlled self-renewal and differentiation of human embryonic stem cells. Proc Natl Acad Sci U S A 2007;104:11298–303 [PubMed: 17581871]
45. Li Z, Leung M, Hopper R, Ellenbogen R, Zhang M. Feeder-free self-renewal of human embryonic stem cells in 3D porous natural polymer scaffolds. Biomaterials 2010;31:404–12 [PubMed: 19819007]
46. Serebriiskii I, Castello-Cros R, Lamb A, Golemis EA, Cukierman E. Fibroblast-derived 3D matrix differentially regulates the growth and drug-responsiveness of human cancer cells. Matrix Biol 2008;27:573–85 [PubMed: 18411046]
47. Nyga A, Cheema U, Loizidou M. 3D tumour models: novel in vitro approaches to cancer studies. J Cell Commun Signal 2011;5:239–48 [PubMed: 21499821]
48. Olgen, S; Overview on Anticancer Drug Design and Development.. Curr Med Chem. 2017.

49. Seliktar D Designing cell-compatible hydrogels for biomedical applications. Science 2012;336:1124–8 [PubMed: 22654050]
50. Lutolf MP. Biomaterials: Spotlight on hydrogels. Nat Mater 2009;8:451–3 [PubMed: 19458644]
51. Wan J, Wen D, Dong L, Tang J, Liu D, Liu Y, et al. Establishment of monoclonal HCC cell lines with organ site-specific tropisms. BMC Cancer 2015;15:678 [PubMed: 26459277]
52. Nikolic M, Sustersic T, Filipovic N. In vitro Models and On-Chip Systems: Biomaterial Interaction Studies With Tissues Generated Using Lung Epithelial and Liver Metabolic Cell Lines. Front Bioeng Biotechnol 2018;6:120 [PubMed: 30234106]
53. Imamura Y, Mukohara T, Shimono Y, Funakoshi Y, Chayahara N, Toyoda M, et al. Comparison of 2D- and 3D-culture models as drug-testing platforms in breast cancer. Oncol Rep 2015;33:1837–43 [PubMed: 25634491]
54. Ledgerwood LG, Kumar D, Eterovic AK, Wick J, Chen K, Zhao H, et al. The degree of intratumor mutational heterogeneity varies by primary tumor sub-site. Oncotarget 2016;7:27185–98 [PubMed: 27034009]
55. Izumchenko E, Paz K, Ciznadija D, Sloma I, Katz A, Vasquez-Dunddel D, et al. Patient-derived xenografts effectively capture responses to oncology therapy in a heterogeneous cohort of patients with solid tumors. Ann Oncol 2017;28:2595–605 [PubMed: 28945830]

Significance:

A lung organoid that exhibits characteristics of a normal human lung is developed to study the biology of metastatic disease and therapeutic intervention.

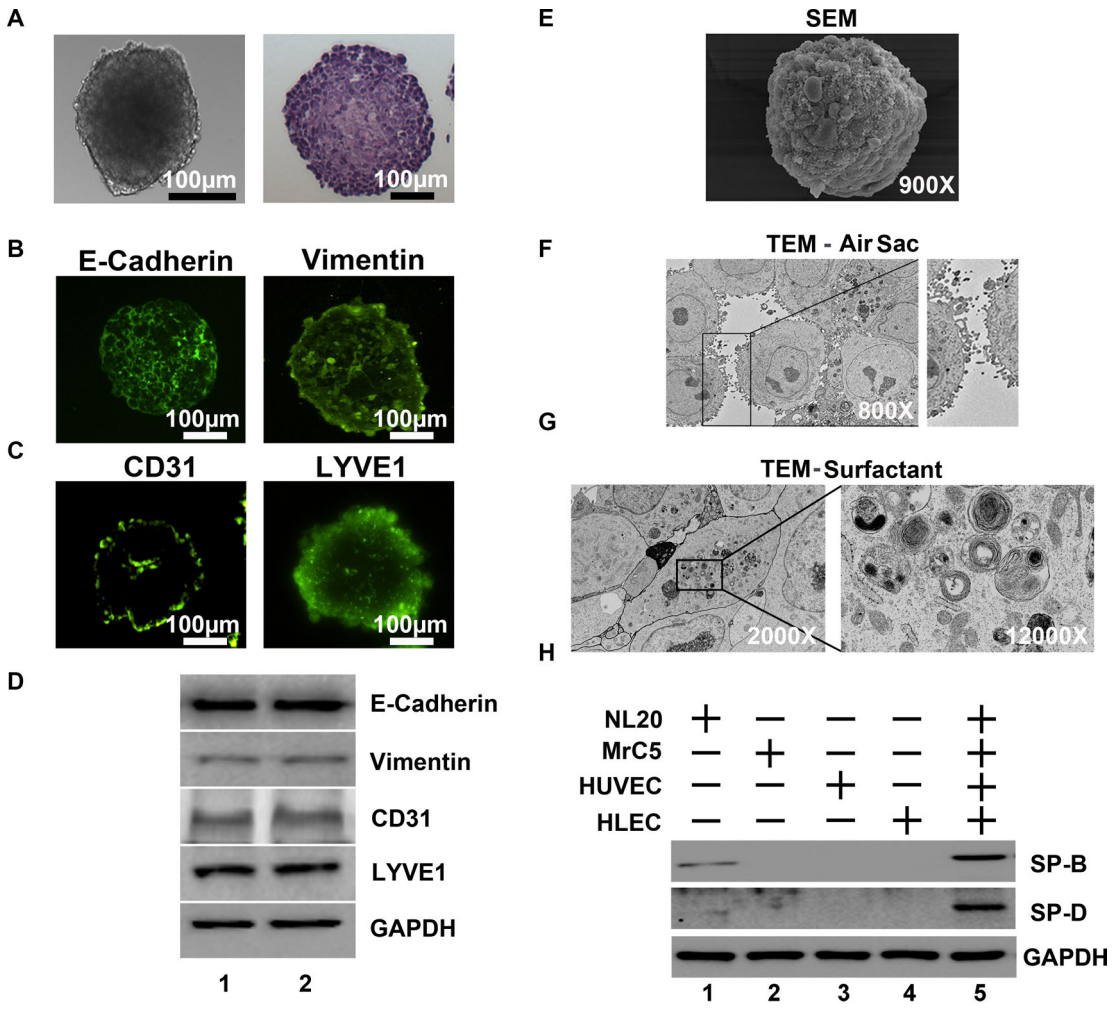

Fig. 1.

Primitive Lung in a Dish (PLiD) culture *in vitro* demonstrates lung air sac architecture. (A) Bright field image (100μm magnification) depicts a 3D PLiD organoid consisting of NL20 (normal human lung epithelial), MrC5 (human normal lung fibroblast), HUVEC (human umbilical vein endothelial cells) and HLEC (human lymphatic endothelial cells) co-cultured in ultralow attachment plates for 5 days. (B) H&E staining. (C) Immunocytochemical characterization of PLiD demonstrates expression of CD31 (endothelial cell marker), LYVE1 (lymphatic endothelial cell marker), vimentin (fibroblast marker) and E-cadherin (epithelial marker). H&E stained section of paraffin embedded PLiD demonstrates a solid mass of cells growing in the organoid. (D) Western blot analyses of 2 representative PLiD cultures demonstrates expression of various cell type markers, epithelial cells (E-Cadherin), fibroblasts (vimentin), HUVEC cells (CD31) and lymphatic endothelial cells (LYVE1). (E) Scanning electron microscopy (SEM) on an individual PLiD organoid at 900X magnification. (F) Transmission electron microscopy (TEM) of PLiD organoid cultures at 800X magnification shows air sac-like structures with microvilli and membrane blebs on the apical surface of epithelial cells typical of lung microarchitecture. (G) TEM image demonstrates surfactant protein like lamellar bodies in PLiD. Well-developed organelles consisting of strands of lipid surrounding multiple disorganized vesicles or lamellar bodies

are observed. (H) Western blot of individual cell types demonstrates expression of SPB and SPD by lung epithelial cells NL20 but not by other cell types used to generate the PLiD. Expression levels of both proteins were elevated in PLiD cultures.

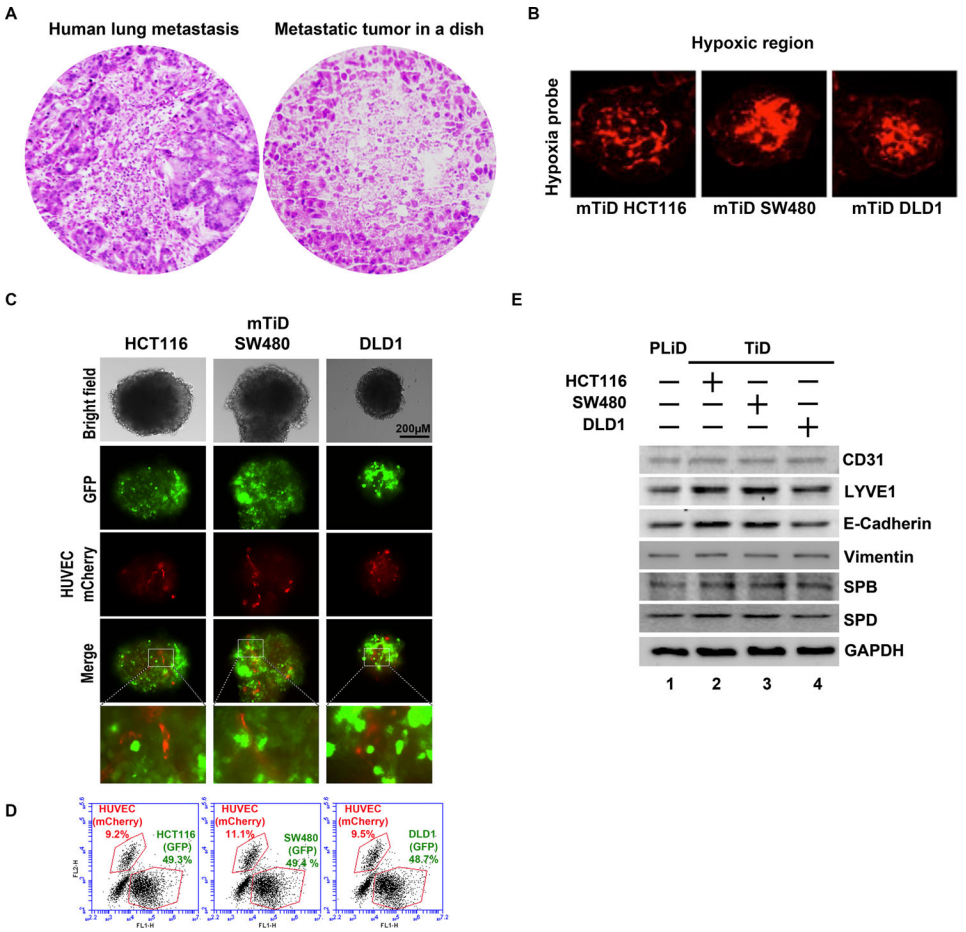

Fig. 2.

(A) The architecture of mTiD cultures resemble that of metastatic tumor in the lung of patients. H&E stained sections of metastatic colon tumor in the lung compared to a mTiD organoid demonstrates micrometastatic tumor deposits. (B) mTiD cultures have a hypoxic core. A) mTiD-HCT116, B) mTiD-SW480 and C) mTiD-DLD1 cultures were stained with Hypoxyprobe-Red549. Hypoxic regions (red) were observed in the core of the organoids. (C) GFP labeled HCT116, SW480 or DLD1 colon cancer cells were grown in presence of PLiD consisting of NL20, MrC5, HLEC and mCherry labeled HUVEC cells. Fluorescence imaging demonstrates distribution of colon cancer (green) and HUVECs (red) in mTiD organoids. Merged images show blood vessel-like tubules of red HUVEC cells in the mTiD. **(D)** Flow cytometry shows the percentage of GFP labeled colon cancer and m-Cherry labeled HUVEC- cells mTiD cultures. (E) Western blot analyses demonstrate the expression of CD31, LYVE1, E-cadherin, vimentin, SPD and SPB in PLiD (devoid of cancer cells) and mTiD cultures.

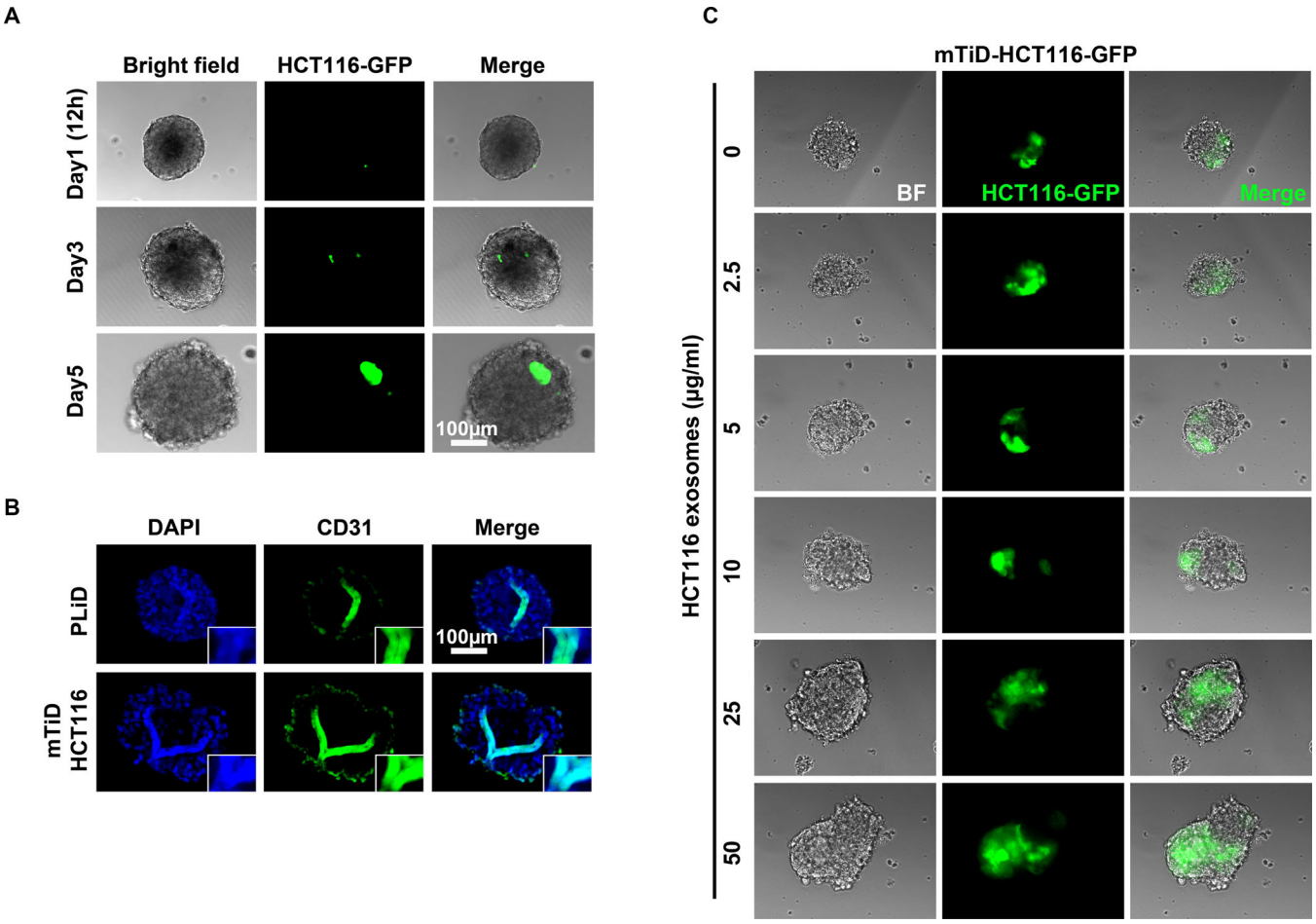

Fig. 3.

Colonization and angiogenesis in mTiD organoids. (A) Live cell imaging shows colonization of HCT116-GFP cells in PLiD live culture in time dependent manner. (B) Immunocytochemical staining shows CD31 positive staining appears like single tube-like formation in PLiD section and mTiD sections. (C) Pretreatment of PLiD with increasing concentrations of cancer cell derived exosomes enhances colonization by cancer cells.

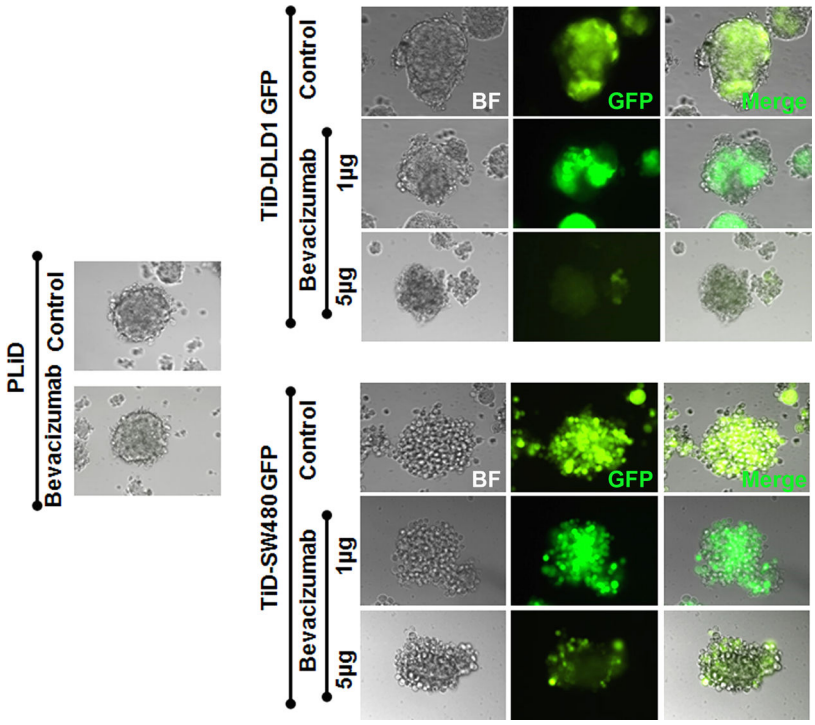

Fig. 4.

Anti-VEGF antibody Bevacizumab suppresses cancer cell growth in mTiD organoids. Dose dependent suppression of GFP-labeled SW480 and DCLK1 cells by Bevacizumab. The antibody does not affect PLiD cultures.

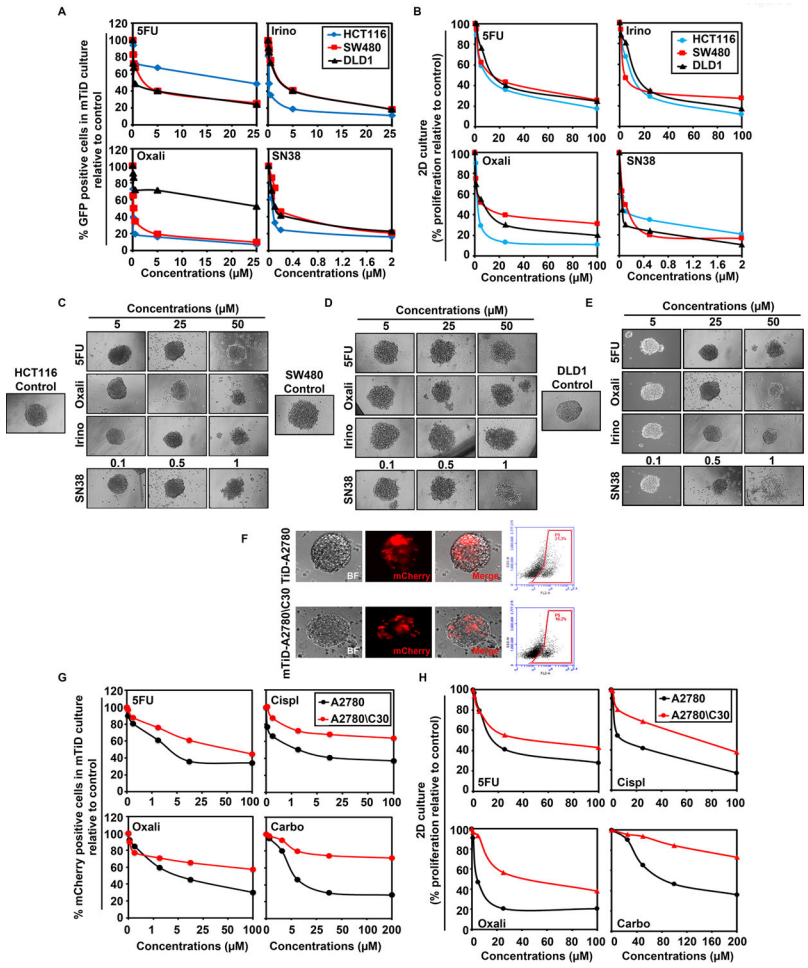

Fig. 5.

Metastatic Tumor-in-a-Dish (TiD) organoids offer a novel drug testing platform. (A) Dose-response curves for colon cancer cells HCT116, SW480 and DLD1 in mTiD cultures after 72 h of exposure to 5FU, irinotecan, oxaliplatin or SN38 are depicted. HCT116 cells were less sensitive to 5FU and DLD1 were less sensitive to oxaliplatin compared to the other agents. IC50 values were determined in dissociated mTiD cultures after 72 h of drug treatment by flow cytometry for GFP-positive colon cancer cells. (B) Colon cancer cell lines grown in 2D are sensitive to chemotherapy agents. HCT116, SW480 and DLD1 were grown in 2D culture and treated with 5FU, Oxaliplatin, Irinotecan or SN38 for 72 h. Cytotoxicity was assessed using hexosaminidase assay. Dose and time dependent cytotoxicity was observed in all three cell lines. IC50 values of colon cancer cells in 2D cultures in response to chemotherapeutic agents over 72 h are depicted. IC50 values were determined in 2D cultures using the hexosaminidase assay. (C) HCT116, (D) SW480 or (E) DLD1 were grown as single cell type 3D cultures and treated with chemotherapeutic agents. Brightfield images were captured after 72 h. (F) mTiD organoids containing mCherry-labeled ovarian cancer cell lines A2780 or A2780/C30-mCherry were imaged by bright field and immunofluorescence. Flow sorted mTiD cultures demonstrate 21.3 to 16.2% tumor (right panels). (G) mTiD-ovarian cancer cells were treated with 5FU and platinum drug (cisplatin, oxaliplatin and carboplatin) for 72 h. A2780\C30 cells are resistant to all the agents

compared to A2780. (H) A2780 and A2780/C30 were grown in 2D cultures and treated with 5FU, cisplatin, oxaliplatin and carboplatin for 72 h. Cytotoxicity was assessed using hexosaminidase assay. Dose and time dependent cytotoxicity was observed in both cell lines.

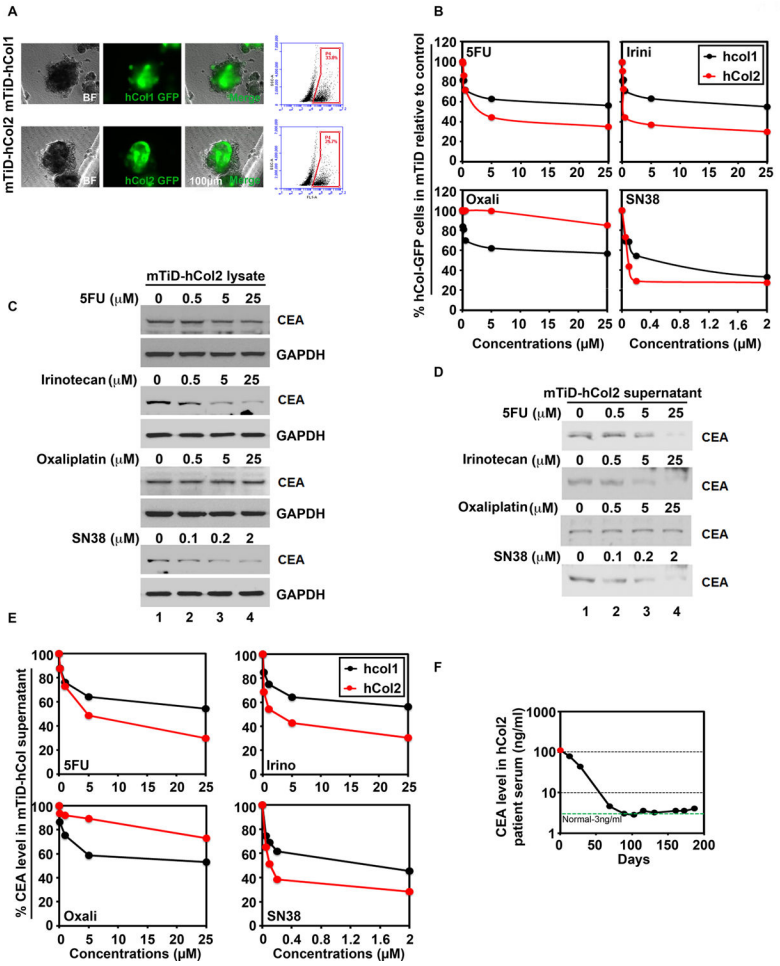

Fig 6.

mTiD is an effective platform to screen drug responses in primary patient-derived colon cancer cells. (A) Representative bright field (BF), GFP-positive cells and merged images of mTiD generated with GFP-labeled primary colon cancer cells isolated from 2 patients (hCol1 and hCol2) are shown. Enzymatically dissociated primary colon mTiD were flow sorted for GFP-positive cells. The mTiD cultures contained 25.7 to 33.8% tumor. (B) Dose-response curves were generated for GFP-labeled primary colon cancer cells in mTiD cultures, after 48h treatment with 5FU, oxaliplatin, irinotecan or SN38 followed by flow sorting. (C) Reduction in carcinoembryonic antigen (CEA) levels in primary colon mTiD cultures corresponds to decrease in serum CEA from the same patient. The hCol1 mTiD cultures were assessed for CEA levels using western blotting of cell lysates and, (D) cell supernatants after treatment with varying doses of 5FU, oxaliplatin (Oxa), irinotecan (Iri), or SN38. (E) Chemiluminescence immunoassay (CLIA) of supernatants from mTiD-hCol2 cultures demonstrates a decrease in CEA levels upon 5FU, Iri and SN38 treatments but not oxaliplatin. (F) CEA levels were measured by CLIA in hCol2 patient serum after chemotherapeutic (FOLFIRI) treatment. Data shows significant linear decrease in CEA serum levels after FOLFIRI treatment.

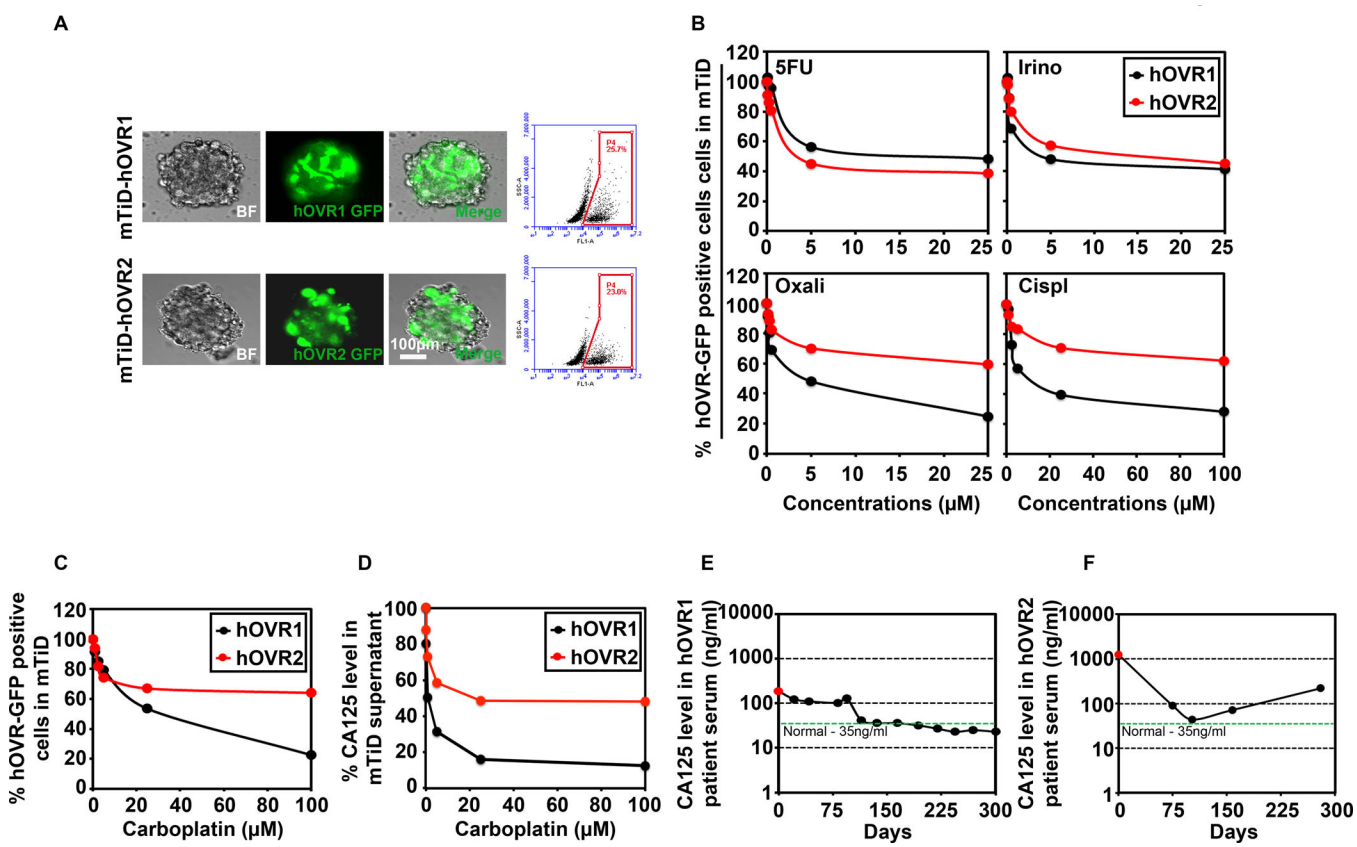

Fig 7.

mTiD is an effective platform to screen drug responses in primary patient-derived ovarian cancer cells. (A) Representative bright field (BF), GFP-positive cells and merged images of mTiD generated with GFP-labeled primary ovarian cancer cells isolated from 2 patients (hOVR1 and hOVR2) are shown. Enzymatically dissociated primary colon mTiD were flow sorted for GFP-positive cells. The mTiD cultures contained 23 to 25.7% tumor. (B) Dose-response curves were generated for GFP-labeled primary ovarian cancer cells in mTiD cultures, after 72 h treatment with 5FU, oxaliplatin, irinotecan or cisplatin followed by flow sorting. 5FU and irinotecan reduced the number of GFP positive hOVR1 and 2 cells. Cisplatin and oxaliplatin reduced the number of hOVR1 cells but not hOVR2 by over 50%. (C) mTiD cultures of GFP-labeled hOVR cells were treated with carboplatin for 72h followed by flow cytometry. hOVR1 (black line) were more sensitive to carboplatin at increasing concentration than hOVR2 cells (red line). (D) Chemiluminescence immunoassay (CLIA) for CA125 in supernatants from mTiD-hOVR1 demonstrated a greater reduction in CA125 levels than mTiD-hOVR2 cultures upon carboplatin treatment. (E) CA125 levels are reduced in the serum from hOVR1 patient responsive to carboplatin treatment. (F) CA125 levels in carboplatin refractory patient hOVR2 showed higher levels of CA125 in the serum.